

# Laser dynamics and relative timing jitter analysis of passively synchronized Er- and Yb-doped mode-locked fiber lasers

Shang-Ying Wu,<sup>1,\*</sup> Wei-Wei Hsiang,<sup>2</sup> and Yinchieh Lai<sup>1,3</sup>

<sup>1</sup>*Department of Photonics and Institute of Electro-Optical Engineering, National Chiao-Tung University, Hsinchu 30010, Taiwan*

<sup>2</sup>*Department of Physics, Fu Jen Catholic University, Taipei 24205, Taiwan*

<sup>3</sup>*Research Center for Applied Sciences, Academia Sinica, Taipei 11529, Taiwan*

\*Corresponding author: sywu123.eo99g@nctu.edu.tw

Received March 6, 2014; revised May 6, 2014; accepted May 6, 2014;  
posted May 7, 2014 (Doc. ID 207639); published June 11, 2014

Passively synchronized Er-doped and Yb-doped mode-locked fiber lasers with a master–slave configuration are theoretically investigated based on the pulse propagation model for simulating pulse collision in the common fiber section and on the master equation model for simulating laser dynamics. Computational results indicate that the central optical frequency of the slave Er laser will be shifted by the significant cross phase modulation (XPM) effect for the laser to become synchronized with the injected master Yb laser pulse train. Pulse duration change caused by fiber dispersion in the common fiber section will distort the ideal anti-symmetric characteristics of the XPM-induced frequency shift versus the relative timing position of the two color pulses. The relative timing jitter noises of the two synchronized lasers can be minimized by adjusting the relative pulse timing position, and the predicted dependence agrees well with the experimental observation. © 2014 Optical Society of America

*OCIS codes:* (140.4050) Mode-locked lasers; (140.3510) Lasers, fiber; (190.7110) Ultrafast nonlinear optics; (270.2500) Fluctuations, relaxations, and noise.  
<http://dx.doi.org/10.1364/JOSAB.31.001508>

## 1. INTRODUCTION

Ultra-low timing synchronization between two independent ultra-short mode-locked laser sources has many advantages for applications including the high-precision measurement, coherent pulse synthesis, precision timing distribution, and photonic analog-to-digital conversion [1]. In these applications, the laser timing jitter has negative influences on the sampling accuracy and will place limitations on the dynamic measurement range or the bit-error-rate performance. In the category of active synchronization techniques, precision pulse timing detection combined with high-speed electronic feedback control of the cavity length is utilized to achieve the synchronization [1,2]. On the other hand, in the category of passive synchronization techniques, the instantaneity of optical cross phase modulation (XPM) effect is utilized as the high-speed synchronization mechanism with a shared cavity or pulse injection configuration [3,4]. In the present work, we choose to consider the pulse injection configuration in favor of its simplicity compared to the cavity-sharing configuration. We also choose to consider the synchronization of an Er fiber laser at 1.5  $\mu\text{m}$  and a Yb fiber laser at 1  $\mu\text{m}$ , in view of their important application for difference frequency generation in the mid-infrared [5]. The synchronization of the fiber lasers can be achieved through the pulse collision inside a shared fiber section. For modeling the two color pulses co-propagation problems, the coupled nonlinear Schrödinger equation (CNLSE) is employed [6,7]. There have been several approaches developed to solve the nonlinear Schrödinger equation (NLSE) type problems efficiently, such as the

split-step Fourier method (SSFM), which is based on the first order approximation of Baker–Campbell–Hausdorff formula [8], and the fourth-order Runge–Kutta in interaction picture (RK4IP) method, which is based on the interaction picture (IP) concept used in quantum mechanics and the RK4 algorithm [9]. Recently the RK4IP method has been performed to obtain excellent computational accuracy for sophisticated light propagation problems. Examples include the super-continuum generation in optical fibers [10] and the optical fiber propagation problems with random birefringence effects [11]. This is the numerical approach we will use in the present work. Furthermore, since the theoretical modeling for the relative timing jitter of passively synchronized two-color lasers can greatly help the understanding and improvement of their performance, it is the objective of the present work to carry out the relative timing jitter noise analysis for observing its physical dependence.

For an individual passively mode-locked laser, an analytical noise model has been developed by Haus and Mecozi based on the soliton perturbation theory [12]. The theory is generalized to active amplitude modulation (AM) and phase modulation (PM) mode-locked lasers in a later paper [13]. A numerical model for investigating the timing jitter of mode-locked lasers has been developed by Paschotta [14,15]. There are also various reported experimental results on the passively mode-locked Er fiber lasers [16,17] and Yb fiber lasers [18,19]. In principle, the timing jitter directly induced by the amplified spontaneous emission noises and indirectly induced through the center frequency fluctuations can be reduced by

the benefits of shorter pulse-width and smaller net intracavity dispersion, respectively. The laser dynamics may also affect the timing jitter under the same net cavity dispersion. Examples include the Yb-doped fiber lasers operated in the self-similar regime showing larger timing jitter than those operated in the stretched-pulse regime [18]. In contrast, for passively synchronized mode-locked fiber lasers, theories for their relative timing jitter noises are still needed to be developed.

In this paper, we first numerically investigate the optical frequency shift induced by the significant XPM effect when the two color pulses collide in the common fiber section. This is accomplished by employing the RK4IP method to simulate cautiously the pulse propagation characteristics caused by fiber dispersion effects and nonlinear effects. The effective center frequency shift is a function of the relative timing position of the two color pulses before the collision. For the pulse injection configuration, we only need to consider the Er laser under the influence of the Yb laser. The dynamics of this passively synchronized Er laser can be simulated by using the master equation model in combination with the above pulse co-propagation model. Additionally, to theoretically analyze the relative timing jitter properties, we derive the evolution equations for the characteristic pulse parameters from the variational solution of the master equation model [20]. The basic equations for the frequency fluctuations and timing position fluctuations are further derived based on the linearization approach around the steady state solution. Finally, the calculated relative jitter noise results are compared with the experimental results to confirm the predicted dependence [21–23].

## 2. LASER DYNAMICS OF PASSIVELY SYNCHRONIZED TWO-COLOR FIBER LASERS

### A. Laser Configuration

The schematic of the considered passively synchronized Er and Yb mode-locked fiber lasers is illustrated in Fig. 1 [21–24]. Both fiber lasers are assumed to be passively mode-locked by using the polarization additive pulse mode-locking (P-APM) technique. Part of the master Yb laser (1.03  $\mu\text{m}$ ) output is employed to perform the pulse injection into the slave Er laser

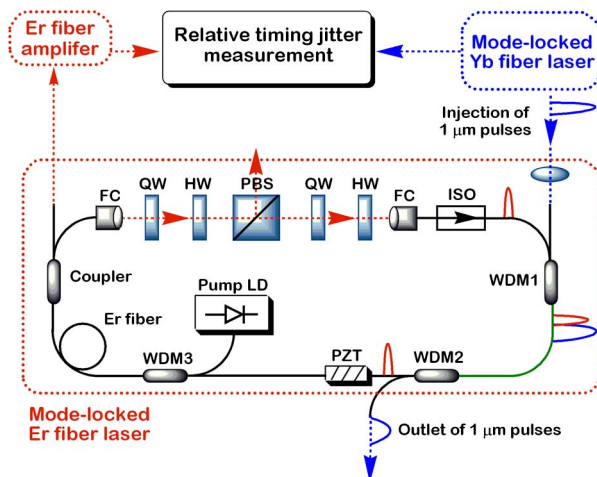


Fig. 1. Schematic of the synchronized laser system. LD, laser diode; WDM, wavelength division multiplexer (WDM1 and WDM2, 1560/1030 nm; WDM3, 1560/976 nm); ISO, isolator; PBS, polarization beam splitter; FC, fiber collimator; QWP, quarter-wave plate; HWP, half-wave plate; PZT, piezoelectric transducer.

(1.56  $\mu\text{m}$ ). Therefore, the 1.03  $\mu\text{m}$  pulses can interact with 1.56  $\mu\text{m}$  pulses through the nonlinear XPM effects for achieving synchronization via the common single-mode fiber section located between WDM1 and WDM2. Experimentally, the relative timing jitter of the two color lasers can be measured based on the nonlinear optical cross correlation method [1,22]. The relative timing position between the 1.56 and 1.03  $\mu\text{m}$  pulses before collision can be adjusted through the control of the piezoelectric transducer (PZT).

### B. Numerical Methods for Modeling the Pulse Co-Propagation

Since the pulse injection configuration is considered, we have to deal efficiently with the nonlinear optical and linear dispersion effects in the common fiber section. The two color pulse interaction can be conveniently described with the following Dirac notation. Namely, given the two color pulse fields  $u_1$  and  $u_2$ , the joint field can be denoted as  $|u\rangle = (u_1, u_2)^T$ . The CNLSE can then be compactly expressed as follows:

$$\frac{\partial}{\partial z}|u\rangle + \hat{\beta}_1 \frac{\partial}{\partial t}|u\rangle - \frac{j}{2}\hat{\beta}_2 \frac{\partial^2}{\partial t^2}|u\rangle + j\hat{n}|u\rangle = 0. \quad (1)$$

Here the physical meanings of the operators  $\beta_1$ ,  $\beta_2$ , and  $n$  are the first order dispersion regarding the inverse group velocity difference, the second order dispersion regarding the pulse broadening, and the nonlinear Kerr effects, respectively. Exact definition of these operators is given below:

$$\hat{\beta}_i = \begin{pmatrix} \beta_{i,u_1} & 0 \\ 0 & \beta_{i,u_2} \end{pmatrix}, \quad i = 1 \text{ or } 2 \quad (2a)$$

and

$$\hat{n} = \begin{pmatrix} \gamma(|u_1|^2 + 2|u_2|^2) & 0 \\ 0 & \gamma(|u_2|^2 + 2|u_1|^2) \end{pmatrix}. \quad (2b)$$

Here,  $\beta_i$  and  $\gamma$  are the dispersion and nonlinear coefficients. Both the SPM and XPM effects are considered in the nonlinear operator term. For the RK4IP numerical algorithm [9,10], we will introduce the dispersion  $\hat{D}$  and nonlinear  $\hat{N}$  operators from Eq. (1) as follows:

$$\hat{D} = -\hat{\beta}_1 \frac{\partial}{\partial t} + \frac{j}{2}\hat{\beta}_2 \frac{\partial^2}{\partial t^2}; \quad \hat{N} = -j\hat{n}. \quad (3)$$

By utilizing the IP transform  $|u\rangle_I = \hat{I}^\dagger(z, z_0)|u\rangle$ , the CNLSE can be formally written as

$$\frac{\partial}{\partial z}|u\rangle_I = \hat{N}_I|u\rangle_I, \quad \hat{N}_I = \hat{I}^\dagger(z, z_0)\hat{N}\hat{I}(z, z_0), \quad (4)$$

where

$$\hat{I}(z, z_0) = \exp((z - z_0)\hat{D}).$$

The differential Eq. (4) can be numerically solved with typical explicit schemes like the fourth-order Runge-Kutta method. The dispersion operator is evaluated in the frequency domain, and the necessary number of FFTs is reduced down to 16 FFTs per step in the present coupled equation case. To be more explicit, the algorithm with the fourth order formula evolves  $|u(z, t)\rangle$  to  $|u(z + h, t)\rangle$  with a spatial step  $h$ . If

represented in the normal picture, the evolved  $|u(z + h, t)\rangle$  is given below:

$$|u\rangle_I = \exp\left(\frac{\hbar\hat{D}}{2}\right)|u(z, t)\rangle \quad (5a)$$

$$|k_1\rangle = \exp\left(\frac{\hbar\hat{D}}{2}\right)[\hbar\hat{N}|u(z, t)\rangle] \quad (5b)$$

$$|k_2\rangle = \hbar\hat{N}\left(|u\rangle_I + \frac{|k_1\rangle}{2}\right) \quad (5c)$$

$$|k_3\rangle = \hbar\hat{N}\left(|u\rangle_I + \frac{|k_2\rangle}{2}\right) \quad (5d)$$

$$|k_4\rangle = \hbar\hat{N}\exp\left(\frac{\hbar\hat{D}}{2}\right)(|u\rangle_I + |k_3\rangle) \quad (5e)$$

$$|u(z + h, t)\rangle = \exp\left(\frac{\hbar\hat{D}}{2}\right)\left(|u\rangle_I + \frac{|k_1\rangle + 2|k_2\rangle + 2|k_3\rangle}{6}\right) + \frac{|k_4\rangle}{6}. \quad (5f)$$

There is a local error of fifth order in the above formula, and hence in general it is a fourth-order accurate scheme. The algorithm can provide sufficient precision to calculate the nonlinear effects of the pulse collision. From our testing computation and previous reports [9,10], employing a higher order scheme like the fourth-order Runge-Kutta in interaction picture (RK4IP) method indeed helps to efficiently obtain more precise results under the nonlinear optical effects. This is because the numerical convergence rate as a function of the step size may not be steep enough for lower order schemes, which will lead to a too small step size for achieving high accuracy.

### C. Induced Frequency Shifts of the Pulse Collision

For checking the accuracy of our numerical model regarding the induced center frequency shifts of significant XPM effects, we first compare with the known analytic frequency-chirp model based on the Gaussian pulse ansatz and with the exclusion of the SPM and GVD effects [24]. By using the same parameters considered in [24], the calculated center wavelength shift of the green pulse versus the relative timing position is shown in Fig. 2(a). The initial green pulse is with 25 ps, 1 nJ, and the infrared pulse is with 33 ps, 70.22 nJ. Parameters for their assumed co-propagating fibers are listed in Table 1. Our computational results evaluated by the phase derivative (the blue line) and by the expected value definition  $E[\lambda] = \int \lambda |\Psi(\lambda)|^2 d\lambda / \int |\Psi(\lambda)|^2 d\lambda$  (the black line) both agree very well with the known results.

After the above checking, we then begin to consider the dispersion and SPM effects based on the parameters of our assumed common fiber (HI-1060), as listed in Table 1. It should be noted that the group velocity difference is experimentally determined based on our previous work [4], and the frequency shifts are evaluated by the expected value method. Employed pulse durations and pulse energies are 0.2 ps and 0.2 nJ for the Er laser and 0.2 ps, 0.74 nJ for the Yb laser, respectively. The single-pass-induced center frequency shift as a function of the relative timing positions ( $t_0 = t_{0,Er} - t_{0,Yb}$ ) is plotted in Fig. 2(b), which is not exactly anti-symmetric, as in the case

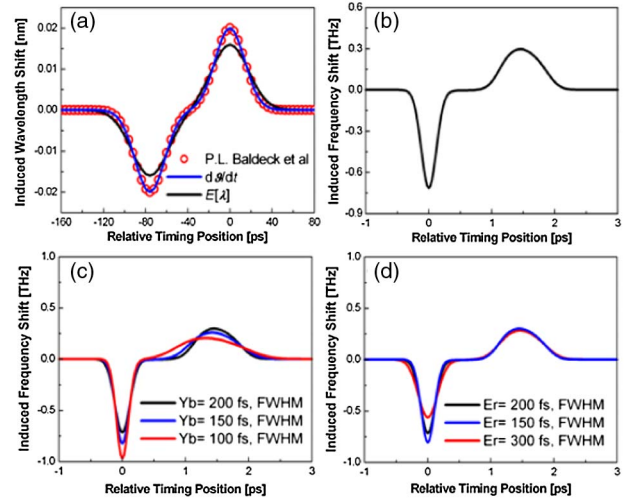


Fig. 2. (a) Comparison of calculated XPM-induced center wavelength shifts of green pulses in [24] (without GVD and SPM) as a function of the input relative timing position between green pulses and infrared pulses. Red circles are analytic results of Baldeck *et al.* [24]. The blue line is our result evaluated by the derivative phase. The black line is our result of  $E[\lambda]$  according to the calculated optical spectrum data. (b), (c), (d) Calculated XPM-induced center frequency shifts of 1.56  $\mu\text{m}$  pulses after the common HI 1060 fiber versus the initial relative timing position between the 1.56 and 1.03  $\mu\text{m}$  pulses. (b) Er,  $\tau_{\text{FWHM}} = 0.2$  ps,  $E_p = 0.2$  nJ, and Yb,  $\tau_{\text{FWHM}} = 0.2$  ps,  $E_p = 0.74$  nJ. (c) Only adjusting Yb,  $\tau_{\text{FWHM}} = 0.2, 0.15, 0.1$  ps. (d) Only adjusting Er,  $\tau_{\text{FWHM}} = 0.2, 0.15, 0.3$  ps.

caused by only the XPM effect. This is due to the pulse duration broadening effect. As shown in Fig. 2(c), when injecting a shorter 1.03  $\mu\text{m}$  pulse, the pulse tends to broaden more in the normal dispersion region, and thus the anti-symmetric characteristics will be distorted more seriously. In contrast, for adjusting the initial pulse duration of the soliton-like 1.56  $\mu\text{m}$  pulse in the anomalous region, the only obvious difference is the peak center frequency change, as seen in Fig. 2(d).

### D. Laser Dynamics of the Synchronized Er-doped Fiber Laser

From the assumption of the pulse injection configuration, we only need to consider the Er laser under the influence of the Yb laser. The master equation for the Er-doped passively mode-locked fiber laser without injecting can be expressed as follows:

$$T_R \frac{\partial u(T, t)}{\partial T} = \left( \frac{g_0}{1 + \int |u|^2 dt / E_s} - l_0 \right) u + (d_r + j d_i) \frac{\partial^2 u}{\partial t^2} + (k_r - j k_i) |u|^2 u. \quad (6)$$

Table 1. Common Fiber Parameters of Numerical Simulations

Type	Optical Fiber <sup>a</sup>		HI1060	
	Infrared	Green	Er	Yb
$\beta_1$ [ps/m]	76	0 <sup>b</sup>	-1.7	0 <sup>b</sup>
$\beta_2$ [ps <sup>2</sup> /m]	0	0	-0.0112	0.0227
$\gamma$ [W <sup>-1</sup> km <sup>-1</sup> ]	2.5	2.5	1.5	1.5

<sup>a</sup>From Baldeck *et al.* [24]

<sup>b</sup>Here by setting  $\beta_1 = 0$ , we have chosen the moving coordinate to be travelling at the group velocity of this wavelength. The  $\beta_1$  in other wavelengths will thus represent the inverse group velocity difference with respect to this wavelength.

The physical meanings for the essential coefficients and their estimated values for generating pulses of  $\sim 0.2$  ps and  $\sim 0.2$  nJ are as follows: unsaturated gain  $g_0 = 4$ ; gain saturation energy  $E_s = 0.047$  nJ; linear loss  $l_0 = 0.8$ ; optical gain bandwidth of 50 nm,  $d_r \approx 2.67 \times 10^{-3}$  g ps<sup>2</sup>,  $g = g_0(1 + \int |u|^2 dt / E_s)^{-1}$ ; net cavity dispersion  $d_i = -0.025$  ps<sup>2</sup>; equivalent fast saturable adsorption by P-APM,  $k_r = 2 \times 10^{-4}$  W<sup>-1</sup>; SPM coefficient  $k_i = 4.55 \times 10^{-3}$  W<sup>-1</sup>; and cavity fundamental repetition frequency  $f_{\text{Rep}} = 43$  MHz. Additionally,  $T$  is the number of the round-trip time and  $t$  is the short time scale. As shown in Fig. 3, the calculated steady state results from the master equation with the RK4IP numerical algorithm and from the pulse parameters evolution equations of our previous work based on the variational analysis under the sech pulse shape ansatz in Eq. (7) [20] agree very nicely with each other. The sech pulse solution ansatz used in the variational method is given by

$$u(T, t) = a(T) \text{sech} \left[ \frac{t - t_0(T)}{\tau(T)} \right]^{1+jC(T)} e^{j\{\omega(T)[t-t_0(T)]+\vartheta(T)\}}. \quad (7)$$

Here  $a(T)$  is the pulse amplitude,  $\tau(T)$  is the pulse-width,  $t_0(T)$  is the pulse timing,  $C(T)$  is the chirp,  $\omega(T)$  is the pulse center frequency, and  $\vartheta(T)$  is the phase.

When considering the injection of the Yb laser pulses for achieving the synchronization, we combine the master equation of the Er laser cavity with the CNLSE pulse propagation model to simulate the laser dynamics. The essential schematic for the numerical modeling procedure is illustrated in Fig. 4. Here the constant timing-shift  $R$  represents the timing walk-off per round-trip caused by the cavity repetition rate difference between the two lasers. It is imposed on the Er laser pulse field after one round-trip calculation to model the cavity mismatch. The Er laser pulse is input to interact with the injected Yb laser pulse in the common fiber section by using the pulse co-propagation model. After the pulse collision, we compensate the fixed time-shift  $\beta_1 L$  induced by the group velocity term in the common HI-1060 fiber of length  $L$  before moving to the master equation model. All the simulation results for demonstrating passive synchronization are essentially obtained by using the RK4IP algorithm. As

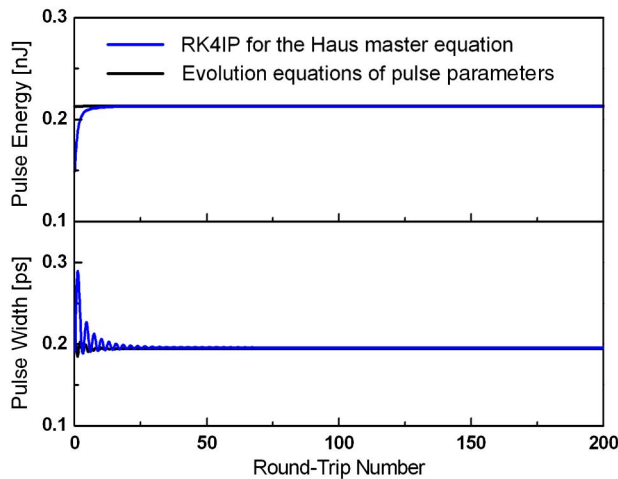


Fig. 3. Comparisons of the calculated results for generating the Er laser of  $\sim 0.2$  nJ pulse-energy and  $\sim 0.2$  ps pulse-width (FWHM) by using the RK4IP algorithm from solving the master equation (the blue lines) and from the evolution equations of the pulse parameters [20] (the black lines).

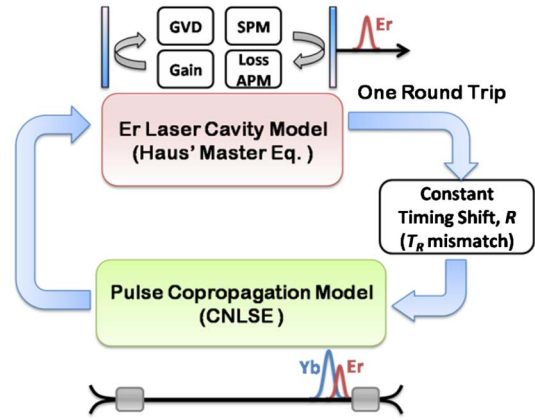


Fig. 4. Schematic of the numerical modeling procedure.

illustrated in Fig. 5(a), we set the Er laser to begin with a timing walk-off of  $-0.8$  ps per round-trip due to the repetition rate difference without the injection. Here the injected Yb laser pulse train is used as the timing reference. When we switch on the Yb laser pulse of  $\sim 0.74$  nJ and  $\sim 0.2$  ps for injection, the Er laser pulse becomes synchronized with the Yb laser pulse quickly to exhibit 0 timing walk-off as in Fig. 5(b). The fundamental dynamics to achieve synchronization can be described as follows. The collision of the Er laser pulse with the injected Yb laser pulse induces some frequency shift via the XPM effect. When the initial repetition rate of the Er laser is higher than that of the Yb laser, for achieving synchronization, the Er laser will require a red-shift of its center frequency to decrease the pulse group velocity in the anomalous dispersion cavity and thus its  $f_{\text{Rep}}$  can be decreased. Since the frequency shift via the XPM is dependent on the relative timing position of the two pulses, the Er laser will tend to get

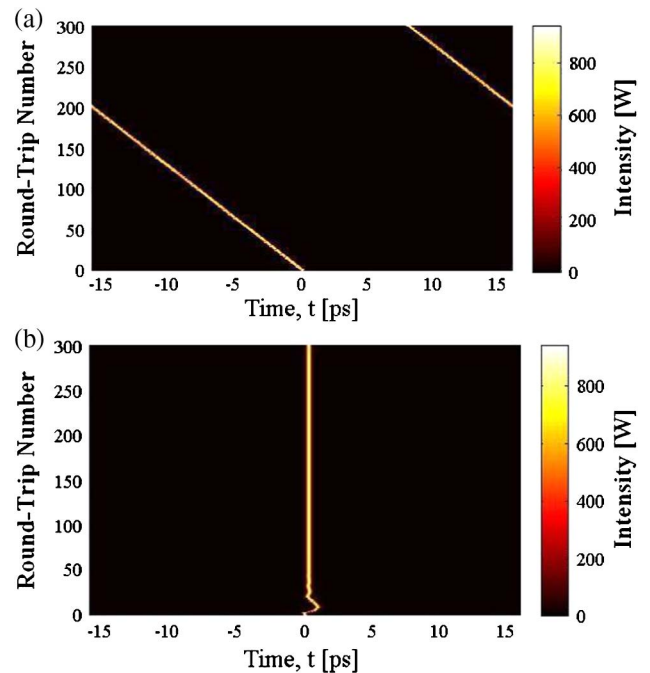


Fig. 5. Calculated results of the  $\sim 0.2$  nJ and  $\sim 0.2$  ps Er laser pulse evolution with the timing walk-off of  $-0.8$  ps per round-trip caused by the cavity repetition rate difference. (a) Unsynchronization without injecting the Yb laser pulse. (b) Synchronization with injecting the Yb laser pulse of  $\sim 0.74$  nJ;  $\sim 0.2$  ps.

stabilized on a suitable relative timing position where the XPM effect can induce the required red-shift. The final steady state center wavelength with injection will be determined by the balance of the XPM effect and the gain filtering effect.

For the above example, the calculated evolution plots for different pulse parameters such as the pulse energy, the pulse-width, the relative timing position, and the center frequency-shift are shown in Fig. 6. It should be noted that the timing position and the center frequency of the Er laser pulse are determined by using the expected value definition. The steady state laser center frequency-shift is smaller than the pulse center frequency-shift after single-pass collision due to the damping effect from the gain filtering, as can be seen from Fig. 6(d). Furthermore, we gradually adjust the value of timing walk-off  $R$  to observe the corresponding variation of the laser operation, especially the relative timing position and the steady state center frequency-shift. The results are shown in Fig. 7. A larger timing walk-off would require a larger center frequency-shift of the Er laser pulse to maintain synchronization. In the above example, the allowable timing walk-off  $R$  is from  $-0.24$  to  $0.27$  ps for achieving synchronization. However, when  $R$  approaches zero, the calculated results are not located smoothly, as shown in the dots region of Fig. 7. We will see in the following relative timing jitter noise analysis that the relative timing jitter noises will also become worse in this regime. Additionally, the XPM-induced center frequency shift function  $m_1(t_0)$  for the Er laser pulse is illustrated in Fig. 8(a) as a function of the initial relative timing positions,  $t_0 = t_{0,\text{Er}} - t_{0,\text{Yb}}$ . The derivative of this function [ $m'_1(t_0)$ ] is also plotted in Fig. 8(b). The importance of  $m_1(t_0)$  and  $m'_1(t_0)$  on the relative timing jitter noises between the two lasers will become clear in the following section.

### 3. RELATIVE TIMING JITTER NOISE ANALYSIS

After successfully modeling the passive synchronization of the two color lasers, we further investigate the relative timing jitter noises between them. By employing the previously mentioned pulse parameters evolution equations from the

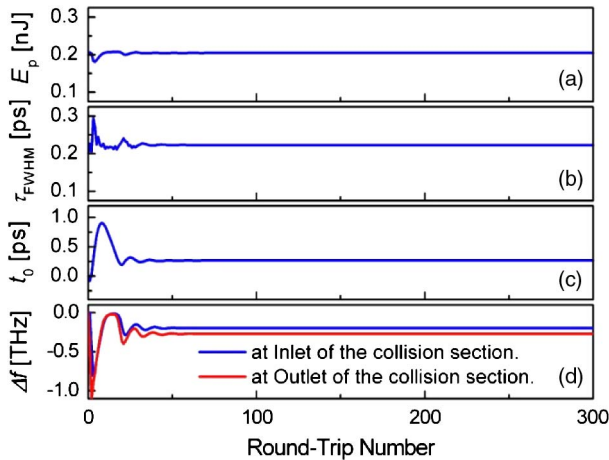


Fig. 6. Calculated evolution plots of the Er laser pulse parameters for achieving the synchronization with the injecting Yb laser pulse train ( $\sim 0.74$  nJ and  $\sim 0.2$  ps) with the initial timing walk-off  $R = -0.8$  ps. (a) Pulse energy. (b) Pulse-width. (c) Relative timing position at the starting of the common fiber. (d) Center frequency shift. Blue lines, at the inlet of the common fiber. Red lines, at the outlet of the common fiber.

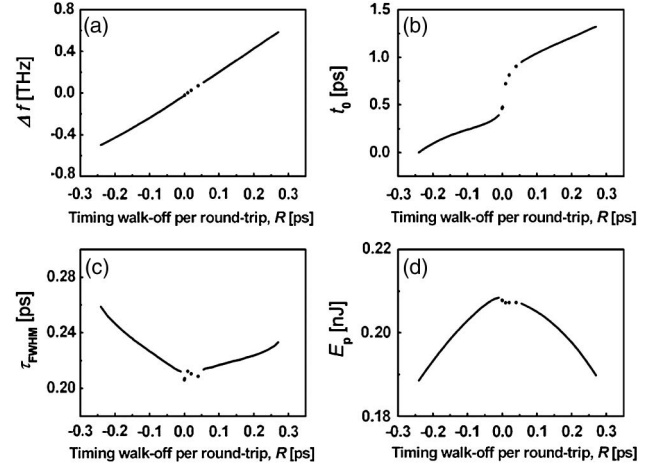


Fig. 7. Calculated steady state results of the Er laser pulse parameters when in synchronization with the injecting Yb laser pulse train. The Yb laser pulse is with  $\sim 0.74$  nJ and  $\sim 0.2$  ps. (a) Frequency shift at the inlet of the common fiber. (b) Relative timing position at the starting point of the common fiber. (c) Pulse-width. (d) Pulse energy.

variational analysis [20] for the Er laser, the coupled equations for the center frequency  $\omega$  and the pulse timing position  $t_0$  can be expressed as below. The new term here is the XPM-induced frequency-shift function  $m_1(t_0)$ :

$$T_R \frac{d\omega}{dT} = m_1(t_0) - \frac{4d_r(1+C^2)}{3\tau^2} \omega \quad (8a)$$

$$T_R \frac{dt_0}{dT} = 2d_i\omega + 2d_rC\omega + R. \quad (8b)$$

To proceed further, we utilize the linearization approach around the calculated steady state solutions of Eqs. (8a) and (8b) to derive the equations for the center frequency fluctuations  $\Delta\omega$  and timing fluctuations  $\Delta t_{0,\text{Er}}$  for the Er fiber-laser. They can be written as below:

$$T_R \frac{d\Delta\omega}{dT} = m'_1(\bar{t}_0)(\Delta t_{0,\text{Er}} - \Delta t_{0,\text{Yb}}) - \frac{4d_r(1+C^2)}{3\tau^2} \Delta\omega + T_R S_\omega(T) \quad (9a)$$

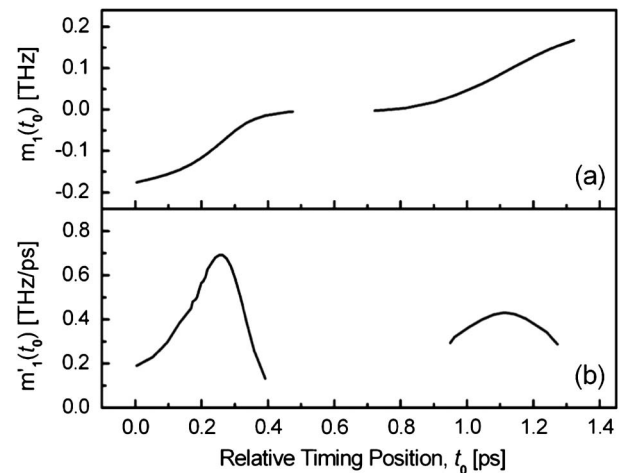


Fig. 8. (a) Induced center frequency shift function  $m_1(t_0)$  of Er laser pulse regarding the initial relative timing positions,  $t_0 = t_{0,\text{Er}} - t_{0,\text{Yb}}$  via the pulse collision effect. The calculation is based on adjusting gradually the timing walk-off  $R$  for synchronizing with injecting the stable  $f_{\text{Rep}}$  Yb laser pulse of  $\sim 0.74$  nJ and  $\sim 0.2$  ps. (b) First-order derivative of the induced frequency shift function,  $m'_1(t_0)$ .

$$T_R \frac{d\Delta t_{0,Er}}{dT} = 2d_i\Delta\omega + 2d_rC\Delta\omega + T_R S_{t_0}(T). \quad (9b)$$

Here both equations are driven by the noise terms  $S_{\omega}(T)$  and  $S_{t_0}(T)$  as in the individual laser case. Additionally,  $m'_1(t_0)$  is the first order derivative of the XPM induced frequency shift function  $m_1(t_0)$ . The calculated  $m'_1(t_0)$  is illustrated in Fig. 8(b). There is the obvious asymmetry of  $m'_1(t_0)$  between the two different operating ranges of the negative and positive  $m_1(t_0)$ . The timing jitter  $\Delta t_{0,Yb}$  of the Yb laser pulse will also have the influences on the Er laser pulse during the collision process in the common fiber section, as seen in the Eq. (9a). The relative timing jitter noise spectrum can be derived from Eqs. (9a) and (9b) analytically with the assumption of a constant chirp parameter  $C$  and by assuming un-correlated noise terms. The final expressions are given below:

$$\begin{aligned} & \langle |\Delta t_{0,Er}(\Omega) - \Delta t_{0,Yb}(\Omega)|^2 \rangle \\ &= \frac{4(d_i + d_r C)^2}{T_R^2 \left[ \left( \Omega^2 + \frac{2(d_i + d_r C)m'_1(t_0)}{T_R} \right)^2 + \left( \frac{\Omega r(1+C^2)}{T_R} \right)^2 \right]} \langle |S_{\omega}(\Omega)|^2 \rangle \\ &+ \frac{\Omega^2 T_R^2 + r^2(1+C^2)^2}{T_R^2 \left[ \left( \Omega^2 + \frac{2(d_i + d_r C)m'_1(t_0)}{T_R} \right)^2 + \left( \frac{\Omega r(1+C^2)}{T_R} \right)^2 \right]} \langle |S_{t_0}(\Omega)|^2 \rangle \\ &+ \frac{\Omega^4 + \left( \frac{\Omega r(1+C^2)}{T_R} \right)^2}{\left[ \left( \Omega^2 + \frac{2(d_i + d_r C)m'_1(t_0)}{T_R} \right)^2 + \left( \frac{\Omega r(1+C^2)}{T_R} \right)^2 \right]} \langle |\Delta t_{0,Yb}(\Omega)|^2 \rangle. \quad (10) \end{aligned}$$

Here  $r$  is defined as a unit-less parameter,  $r = 4d_r/3\tau^2$ . To estimate the quantum-limited timing jitter, the noise terms  $S_{\omega}(T)$  and  $S_{t_0}(T)$  can be assumed to be uncorrelated white noises with the corresponding diffusion coefficients  $D_{\omega}$ , and  $D_{t_0}$  [14]. It should be noted that when  $C$ ,  $m'_1(t_0)$  and  $\Delta t_{0,Yb}$  are ignored, one obtains the same results for an individual passive mode-locked laser [12].

As a numerical example, the relative timing jitter in a root-mean-square sense is calculated by integrating the above spectrum from 1 kHz to half the repetition frequency (21.5 MHz) under the above assumption of the laser cavity parameters. The diffusion coefficients ( $D_{\omega}$  and  $D_{t_0}$ ) are evaluated by using the following parameters: for the Er laser,  $\hbar\omega_c \approx 0.8$  eV,  $T_R \approx 23$  ns, the excess noise factor  $\Theta \approx 10$  and others ( $\tau_{FWHM}$ ,  $g_s$  and  $w_0$ ) from previously calculated results; for the Yb laser,  $\hbar\omega_c \approx 1.2$  eV,  $T_R \approx 23$  ns,  $\Theta \approx 10$ ,  $\tau_{FWHM} \approx 0.2$  ps,  $g_s \approx 0.76$ , and  $w_0 \approx 0.74$  nJ. From experimental observation [18,19], the timing jitter spectrum of a passively mode-locked Yb laser shows the  $\sim 1/f^2$  slope in the low frequency regime probably originated from the pulse timing random walk directly caused by the noises in each round trip and the  $\sim 1/f^4$  slope in the higher frequency regime probably caused by the center frequency fluctuations indirectly. These observations agree with the predictions based on the master equation model for passive mode-locked lasers [12]. However, different lasers may have different scaling factors compared to the ideal quantum noise limited prediction. Therefore in the following calculation, the Yb timing jitter spectrum (under  $d_i \approx 0.0055$  ps<sup>2</sup> and  $d_r \approx 4.33 \times 10^{-4}$  ps<sup>2</sup>) is assumed to be given by the Haus and Mecozzi's model with a scaling excess noise factor  $\Theta$ . It should also be noted that the chirp parameter  $C$  is estimated by using the expected value definition [25] based on the numerically calculated

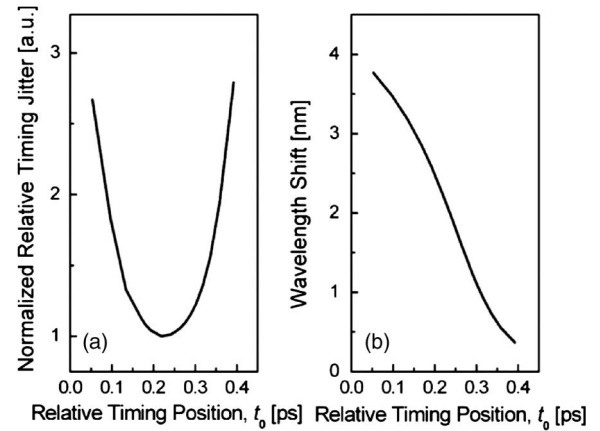


Fig. 9. (a) Calculated relative timing jitter (normalized) versus the relative timing position between the two color pulses in the beginning of the collision. (b) The corresponding center wavelength shift of the Er pulse at the inlet of the common fiber section.

steady state Er pulse solution. One typical result within the red-shift regime is illustrated in Fig. 9(a), where the relative timing jitter shows the dependence on the relative timing position between the two color pulses. The physical reason for this dependence can be seen from Eq. (9a). Because the  $m'_1(t_0)$  term works as a timing-to-frequency feedback term, the relative timing jitter is expected to be suppressed more if the magnitude of  $m'_1(t_0)$  is larger. This dependence can be obviously seen from Eq. (10) and verified by comparing Fig. 9(a) with Fig. 8(b). This important dependence has been observed in our previous experimental work [21,22]. The calculated center wavelength-shift of the Er laser pulse is plotted in Fig. 9(b), which also agrees reasonably with the experimental results monitored at the inlet of the common fiber section [22]. The corresponding lasing wavelength-shift at the point with minimum relative timing jitter is around 2 nm. Additionally, the 3 dB bandwidth of the relative timing jitter can be reduced from a few millihertz to the hundreds kilohertz as shown in Fig. 10 for the  $t_0 \approx 0.218$  ps case. When the chirp approaches zero gradually, a peaking spectrum indicative of a pulse retiming oscillation of the passive synchronization may be revealed.

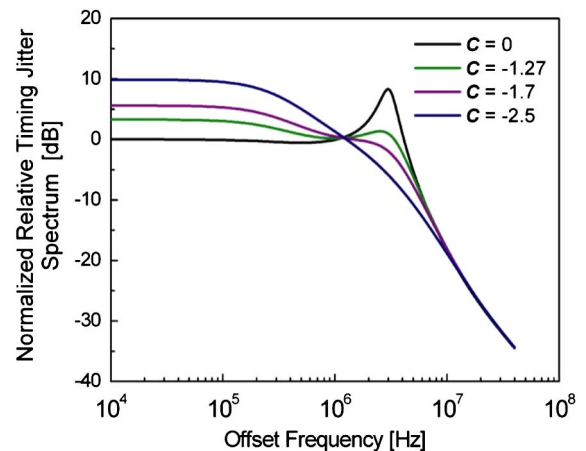


Fig. 10. Normalized relative timing jitter spectrum under the relative timing position  $t_0 \approx 0.218$  ps, for different chirps:  $C \approx 0$  (the black line),  $C \approx -1.27$  (the green line),  $C \approx -1.7$  (the purple line), and  $C \approx -2.5$  (the blue line).

To summarize, by employing the XPM effect for achieving passive synchronization, the relative timing jitter of the two lasers can be suppressed more effectively by appropriately adjusting their cavity length difference. Zero free-running pulse timing walk-off is not the best operating point. One needs to search for the point where the slope of the XPM-induced frequency shift is maximum. For the considered example, the calculated relative timing jitter ( $\sim 0.34$  fs within 1 kHz–21.5 MHz) is reduced by at least a factor of 15 in comparison to that of the individual passive mode-locked fiber laser (Er:  $\sim 5.22$  fs within 1 kHz–21.5 MHz, Yb:  $\sim 5.45$  fs within 1 kHz–21.5 MHz). These results nicely demonstrate the potential advantages of the investigated passive synchronization scheme.

#### 4. CONCLUSION

In conclusion, we have carried out a theoretical study for investigating passively synchronized Er- and Yb-doped mode-locked fiber lasers under the master-slave configuration for the first time. The optical nonlinear interaction of the two-color pulses co-propagating in the common fiber section is simulated by numerically solving the CNLSE with the RK4IP method. The slave passively mode-locked Er fiber laser with the injection of the master Yb laser pulse train is modeled by the master equation model in combination with the pulse propagation model for the common fiber section to determine the steady state pulse solution inside the cavity. The physical mechanism for achieving passive synchronization is made more clear through the modeling. It is found that the nonlinear XPM effect induced by pulse collision causes a frequency shift of the Er laser pulse and the magnitude of the frequency shift is dependent on the relative timing position of the two pulses. This serves as a feedback mechanism from the relative-pulse-timing to the center-optical-frequency and then subsequently to the laser repetition rate through the dispersion effect. Passive synchronization of the two lasers is made possible through such a feedback mechanism, and thus there will be a center optical frequency shift when the synchronization is achieved, which is determined by the balance of the XPM-induced frequency shift and the damping effect of gain filtering. This explains the lasing wavelength shift that has been observed experimentally. After verifying that the passive synchronization of two-color mode-locked fiber lasers can be achieved, we then employ the variational method and the linearization technique to derive the coupled equations for the center frequency and the relative timing position fluctuations from the pulse parameter evolution equations. The relative timing jitter is found to exhibit the dependence on the relative timing position of the two color pulses before the collision. The predicted dependence and the corresponding center optical wavelength shift for the Er laser agree reasonably with our previous experimental observations. The relative timing jitter between the two lasers can be minimized by appropriately adjusting their cavity length difference. The minimized relative timing jitter can be smaller than the timing jitters of individual passive mode-locked fiber lasers by at least a factor of 15 in the considered example. This revealed dependence can provide one flexible approach to further optimize the passively synchronized fiber laser systems for achieving ultra-low timing performances and for developing new applications.

#### ACKNOWLEDGMENTS

This work is supported by the National Science Council of Taiwan under the contract NSC 102-2221-E-009-152-MY3.

#### REFERENCES

1. J. Kim and F. X. Kärtner, "Attosecond-precision ultrafast photonics," *Laser Photon. Rev.* **4**, 432–456 (2010).
2. J. A. Cox, W. P. Putnam, A. Sell, A. Leitenstorfer, and F. X. Kärtner, "Pulse synthesis in the single-cycle regime from independent mode-locked lasers using attosecond-precision feedback," *Opt. Lett.* **37**, 3579–3581 (2012).
3. D. Yoshitomi, Y. Kobayashi, M. Kakehata, H. Takada, K. Torizuka, T. Onuma, H. Yokoi, T. Sekiguchi, and S. Nakamura, "Ultralow-jitter passive timing stabilization of a mode-locked Er-doped fiber laser by injection of an optical pulse train," *Opt. Lett.* **31**, 3243–3245 (2006).
4. W.-W. Hsiang, W.-C. Chiao, C.-Y. Wu, and Y. Lai, "Direct observation of two-color pulse dynamics in passively synchronized Er and Yb mode-locked fiber lasers," *Opt. Express* **19**, 24507–24515 (2011).
5. J. Biegert, P. K. Bates, and O. Chalus, "New mid-infrared light sources," *IEEE J. Sel. Topics Quantum Electron.* **18**, 531–540 (2012).
6. C. Fürst, A. Leitenstorfer, and A. Laubereau, "Mechanism for self-synchronization of femtosecond pulses in a two-color Ti:sapphire laser," *IEEE J. Sel. Topics Quantum Electron.* **2**, 473–479 (1996).
7. A. M. Weiner, *Ultrafast Optics* (Wiley, 2009).
8. O. V. Sinkin, R. Holzöhner, J. Zwick, and C. R. Menyuk, "Optimization of the split-step Fourier method in modeling optical-fiber communications systems," *J. Lightwave Technol.* **21**, 61–68 (2003).
9. J. Hult, "A fourth-order Runge-Kutta in the interaction picture method for simulating supercontinuum generation in optical fibers," *J. Lightwave Technol.* **25**, 3770–3775 (2007).
10. A. M. Heidt, "Efficient adaptive step size method for the simulation of supercontinuum generation in optical fibers," *J. Lightwave Technol.* **27**, 3984–3991 (2009).
11. Z. Zhang, L. Chen, and X. Bao, "A fourth-order Runge-Kutta in the interaction picture method for numerically solving the coupled nonlinear Schrödinger equation," *Opt. Express* **18**, 8261–8276 (2010).
12. H. A. Haus and A. Mecozzi, "Noise of mode-locked lasers," *IEEE J. Quantum Electron.* **29**, 983–996 (1993).
13. M. E. Grein, H. A. Haus, Y. Chen, and E. P. Ippen, "Quantum-limited timing jitter in actively modelocked lasers," *IEEE J. Quantum Electron.* **40**, 1458–1470 (2004).
14. R. Paschotta, "Noise of mode-locked lasers (Part I): numerical model," *Appl. Phys. B* **79**, 153–162 (2004).
15. R. Paschotta, "Timing jitter and phase noise of mode-locked fiber lasers," *Opt. Express* **18**, 5041–5054 (2010).
16. J. Chen, J. W. SICKLER, E. P. Ippen, and F. X. Kärtner, "High repetition rate, low jitter, low intensity noise, fundamentally mode-locked 167 fs soliton Er-fiber laser," *Opt. Lett.* **32**, 1566–1568 (2007).
17. J. A. Cox, A. H. Nejadmalayeri, J. Kim, and F. X. Kärtner, "Complete characterization of quantum-limited timing jitter in passively mode-locked fiber lasers," *Opt. Lett.* **35**, 3522–3524 (2010).
18. Y. Song, K. Jung, and J. Kim, "Impact of pulse dynamics on timing jitter in mode-locked fiber lasers," *Opt. Lett.* **36**, 1761–1763 (2011).
19. Y. Song, C. Kim, K. Jung, H. Kim, and J. Kim, "Timing jitter optimization of mode-locked Yb-fiber lasers toward the attosecond regime," *Opt. Express* **19**, 14518–14525 (2011).
20. W.-W. Hsiang, H.-C. Chang, and Y. Lai, "Laser dynamics of a 10 GHz 0.55 ps asynchronously harmonic modelocked Er-doped fiber soliton laser," *IEEE J. Quantum Electron.* **46**, 292–299 (2010).
21. W.-W. Hsiang, B.-W. Tsai, C. Hu, S.-Y. Wu, and Y. Lai, "Subfemtosecond synchronization between Yb-fiber and Er-fiber lasers by controlling the relative injection timing," in *Conferences*

- on Lasers and Electro-Optics* (Optical Society of America, 2013), paper JTh2A.27.
22. B.-W. Tsai, S.-Y. Wu, C. Hu, W.-W. Hsiang, and Y. Lai, "Subfemtosecond hybrid synchronization between ultrafast Yb- and Er-fiber laser systems by controlling the relative injection timing," *Opt. Lett.* **38**, 3456–3459 (2013).
  23. S.-Y. Wu, W.-W. Hsiang, and Y. Lai, "Relative timing jitter of passively synchronized Er-doped and Yb-doped mode-locked fiber lasers," in *IEEE Photonics Conference* (IEEE Photonics Society, 2013), paper ThB.1.2.
  24. P. L. Baldeck, R. R. Alfano, and G. P. Agrawal, "Induced-frequency shift of copropagating ultrafast optical pulses," *Appl. Phys. Lett.* **52**, 1939–1941 (1988).
  25. N. G. Usechak and G. P. Agrawal, "Rate-equation approach for frequency-modulation mode locking using the moment method," *J. Opt. Soc. Am. B* **22**, 2570–2580 (2005).